

Supporting Information

Hydration and Conformational Mechanics of Single End-Tethered Elastin-Like Polypeptides

Alexei Valiaev, Dong Woo Lim, Scott Schmidler, Robert L. Clark, Ashutosh Chilkoti,

and Stefan Zauscher

Substrate Preparation and ELP Coupling. To minimize unspecific interactions between ELP and a gold surface we used a mixed SAM of oligoethylene-glycol terminated alkanethiols. EG6 thiol with a -COOH terminal group was purchased from Prochimia (Cat. #: TH 011-01). -CH₃ terminated EG3 thiol was custom-synthesized in our laboratory. The concentrated solution of EG6 thiol (as received from Prochimia) and the stock solution of EG3 thiol were diluted in ethanol to a concentration of approximately 1 mM. Both thiols were then mixed together by sonication. Before use, the thiol mixture was kept overnight in dark environment and in a sealed vial. The gold-coated substrates were then placed in the mixed thiol solution overnight (~12 hours) and kept at room temperature and in a dark environment. The functionalized substrates were then sonicated for 3 minutes in ethanol, washed thoroughly with ethanol, and finally dried under a stream of dry nitrogen. The -COOH terminal group of EG6 was activated by reaction for 30 minutes with 1-ethyl-3-(dimethylamino)propyl carbodiimide EDAC (0.1 M, Aldrich) and N-hydroxysuccinimide (NHS) (0.2 M, Aldrich) in Milli-QTM (18 M Ω /cm) water at room

temperature. The substrate samples were then sonicated for 3 minutes in ethanol, washed in ethanol and then in Milli-QTM grade water, and finally dried under a stream of dry nitrogen. A drop of a 1 μM solution of ELP was then pipetted onto the functionalized gold substrate, and incubated for 2-3 hours to covalently conjugate the ELP to the surface. After incubation, the substrate was washed with a 0.05% sodium dodecyl sulfate (SDS, Pierce) solution to desorb unreacted ELP from the surface, and then exhaustively rinsed with PBS and Milli-QTM grade water. The mixed thiol SAM layer had a thickness of 17.6 \pm 0.3 \AA , as determined by ellipsometric measurements in air.

Transition Temperatures for Several ELP Constructs. In Table S1, the transition temperatures for ELP constructs used in this work are listed. The transition temperature is defined at the maximum in the turbidity gradient while heating at 1 $^{\circ}\text{C}/\text{min}$ for an ELP concentration of 25 μM in PBS. The spread is the range between upper and lower thresholds at 25% of the maximum in the turbidity gradient.

Table S1: Transition temperatures for several ELPs.

Experimental construct	Solution Concentration/Condition	Transition Temperature
ELP1-180	PBS (25 μM)	41.0 $^{\circ}\text{C}$ - 41.6 $^{\circ}\text{C}$
	PBS+1M NaCl (25 μM)	\sim 25.7 $^{\circ}\text{C}$
	PBS+1.5 M NaCl (25 μM)	17 -18 $^{\circ}\text{C}$
ELP4-120	PBS (25 μM)	28.6 $^{\circ}\text{C}$
ELP2-160	PBS (25 μM)	70.8 $^{\circ}\text{C}$

Data Reduction. For each experimental condition, several thousand force-extension curves were collected. Only a fraction of the measured curves, however, represent the actual single molecule force-extension event of interest. Many exhibit artifacts such as multiple force-extension events, large nonspecific adhesions or simultaneous pulling of several molecules. A custom Matlab program was developed to automatically filter the data based on several criteria established to reject curves that exhibit these artifacts. An important control that we applied was that all of the curves selected for analysis could be normalized by contour length at a constant force.

Values for the fit parameters, such as the Kuhn segment length, obtained by fitting the FJC model to the force-extension data can vary significantly depending on the force range chosen for the fitting.¹⁻³ To remove this ambiguity we choose for all curves a force window between 60 pN and 200 pN for fitting the FJC model. This range was chosen to maximize the force region in which all of the selected curves were well described by the FJC model and to minimize effects from nonspecific interactions at small extensions, and thermal noise fluctuations of the cantilever.

The commonly used approach to fitting polymer elasticity models is least squares (LS) error minimization, assuming a constant variance. However, a plot of the residuals (Fig. S1) which was produced by subtracting the predicted extension, obtained from the FJC model fit to force-extension data below 200 pN, from the experimentally measured extension, shows a clear violation of the constant variance assumption. Observations at low forces are subject to significantly greater thermal fluctuation than those at higher forces, so that noise variance σ^2 decreases with increasing f . Because σ^2 was not constant, maximum likelihood estimates were obtained by a weighted least-squares (WLS) minimization, where the weight factors were found using a Langevin (or von Mises-Fisher) distribution $V_{d(f)}$:⁴

$$V_{d(f)}^2 = n_k l_k^2 \left(1 - L(\beta)^2 - \frac{2}{\beta} L(\beta) \right), \quad (1S)$$

where $L(\beta)$ is the Langevin function defined as $L(\beta) = \coth(\beta) - \frac{1}{\beta}$, with $\beta = \frac{Fl_k}{k_B T}$.

Many force-extension curves are usually recorded during measurements under the same experimental condition. Because each curve represents the same molecular sequence, each provides additional information for estimating the elasticity parameters of the molecule. We now pool information from all of the curves to improve our estimate of l_K and reduce the uncertainty $var(l_K)$ of the estimated parameters. However, the random location of the AFM cantilever tip attachment along the molecule means that each curve has a distinct value of contour length L . We thus need to simultaneously estimate the parameters $\theta = (l_K; L_1, \dots, L_m)$, where l_K is now the common effective Kuhn segment length parameter.

We performed this estimation by stagewise minimization, where l_K was discretized in the range of plausible values (l_K^{\min}, l_K^{\max}) with $\Delta l_K = l_K^s - l_K^{s-1}$. Δl_K was chosen to be about 2 orders of magnitude smaller than a typical mean value of l_K under the same experimental condition. For each value of the Kuhn length, l_K , we find the contour length by minimizing the weighted LS criteria,

$$L_j^s = \arg \min_{L_j} \sum_{i=1}^{n_j} w_{ij} \left(l_K^s, L_j \right) \left(x_{ij} - g(f_{ij}, l_K^s, L_j) \right)^2 - \log w_{ij}, \quad (2S)$$

where w_{ij} is the weight factor, x_{ij} and f_{ij} are the measured separation and force corresponding to the i^{th} data point on the j^{th} curve, L_j is the contour length corresponding to the j^{th} curve and

$g(f_{ij}, l_K^s, L_j)$ is the estimate for separation, obtained from the FJC model. Finally, we minimized over discrete values of l_K according to,

$$\min_{l_K} \sum_{j=1} \min_{L_j} \sum_{i=1} w_{ij} (x_{ij} - g(f_{ij}, l_K, L_j))^2. \quad (3S)$$

We used a nonparametric bootstrap procedure to obtain confidence intervals for the fitted parameters by Monte Carlo resampling⁵. In this procedure the standard error of the parameter estimation is found as (4S),

$$s\hat{e} = \sqrt{\frac{1}{B-1} \sum_{b=1}^B (l_K^b - \bar{l}_K)^2}, \quad (4S)$$

where l_K^b is the value of the Kuhn length estimated from the FJC model at the b^{th} bootstrap,

where $\bar{l}_K = \frac{1}{B} \sum_{b=1}^B l_K^b$ is a parameter average estimated from all bootstrap samples, and where B

is the total number of bootstrap samples.

Copies of the MATLAB scripts are available from the corresponding author upon request.

Hydrodynamic Drag. The pulling rates used in force spectroscopy experiments⁶⁻⁸ are often sufficient to cause hydrodynamic drag forces on the cantilever. This drag force needs to be subtracted from the measured forces if precise estimates for the FJC fit parameters are to be obtained. Since the flow velocities are generally small (viscous flow regime), the drag force, F_H , can be described by:

$$F_H = C\mu V, \quad (5S)$$

where C is a geometry dependent constant, μ is the viscosity, and V is the relative velocity between cantilever and the surrounding fluid phase. To estimate the hydrodynamic drag contribution associated with a particular cantilever type, we performed force measurements at

different sample displacement rates. As expected, the force values obtained from cantilever deflection, depended linearly on displacement rate, which allowed the coefficient ($C\mu$) to be determined, $C \cdot \mu_{Hex} = 24 \frac{\text{pN}}{\mu\text{m/sec}}$ for hexadecane and $C \cdot \mu_{H_2O} = 7 \frac{\text{pN}}{\mu\text{m/sec}}$ for water (Fig. S2).

The ratio of these slopes is 3.43 and compares favorably with the viscosity ratio of 3.76, obtained from the viscosities of hexadecane and water at room temperature ($3.35 \text{ cP}/0.89\text{cP} = 3.76$).

In a typical single molecule pulling experiment, performed at constant displacement rate, the relative speed between cantilever and surrounding fluid changes as the molecule is stretched. To account for this, we estimated the relative cantilever speed by differentiating the measured force-displacement data and then subtracted the drag force, calculated from Eq. 5S, at every point along the measured force-extension curve. A comparison of force-extension curves, obtained for ELP1-180 in PBS + 1.5 M NaCl solution, with and without drag force correction is shown in Figure S3. Although the magnitude of the hydrodynamic drag forces is typically less than the amplitude of the thermal noise fluctuations, it still causes a force offset which affects the Kuhn length predicted by the FJC model.

Effect of Cantilever Spring Constant on Kuhn length. The cantilever spring constant, K_c , is determined from the power spectral density of the thermal noise fluctuations in solution,⁹ and typically has an uncertainty of $\pm 10\%$.⁹⁻¹² This leads to uncertainties in the force determination. To explore the effect of uncertainties in the cantilever spring constant on the Kuhn length distributions, we performed a sensitivity analysis in which we assumed different values for the spring constants. For this analysis we recalculated the force, for each cantilever spring constant, according to Equation 6S:

$$f_{ij} = M \cdot K_c \cdot D_{ij}, \quad (6S)$$

where M is a multiplication factor in the range between 0.8 and 1.2, and where D_{ij} is the deflection of the AFM cantilever (corresponding to the i^{th} curve and the j^{th} data point).

In Figure S4 a), the distributions for ELP1-180 in MQ-grade water at 25 deg. C are shown, and in Figure S4 b), the distributions for ELP1-180 in PBS with 1.5 M NaCl added (at 25 deg. C) are shown. First one can see that the mean and the breadth of the Kuhn length distributions at each of the experimental conditions are not significantly affected by cantilever stiffness variations. Furthermore, comparing these two figures, it is clear that for all combinations of the spring constants, the Kuhn length distributions under these two experimental conditions remain significantly separated and resolvable. Applying similar sensitivity analyses to all experimental conditions, we found that an uncertainty in the spring constant of up to 20% would still render the distributions under all experimental conditions to be statistically different and distinguishable.

Non-parametric Fitting. Instead of using the effective Kuhn segment lengths as a reporter for changes in ELP elasticity and hydration, we also compared our data sets through nonparametric fitting, using the area under the force-extension curves. This area is proportional to the total energy required to stretch the molecule. Again, as in the analysis of the Kuhn segment lengths, we used the force window between 60 and 200 pN to eliminate contributions from unspecific interactions at low extension ratios. For this procedure, we first sorted the normalized force extension curves by separation and then applied a local regression smoothing procedure to fit a set of normalized curves. We then used our bootstrapping procedure, applied to a set of force-

extension curves, to calculate the uncertainty in the area estimation under the smoothed curves. Typical results obtained by using this nonparametric fitting are shown in Figure S5 for one experimental condition.

Effect of Ionic Strength on Conformation of End-Grafted ELPs. To study the effect of monovalent salt (NaCl) addition on the surface conformation of end-grafted ELPs, we performed AFM surface force measurements over a large range of ionic strengths (Fig. S6). In these experiments the tip of a Si_3N_4 cantilever was brought into increasingly stronger compressive contact with surface grafted ELP1-180. Repulsive steric forces arise from the restriction of conformational degrees of freedom in the thermally mobile polypeptide chain. Since experiments were performed in PBS buffer, with various amounts of salt added (further shielding electrostatic interactions), repulsive force contributions due to electric double layer overlap were small and short ranged (less than 1 nm). The force-separation data in Figure S6 suggests that the distal ends of the surface grafted ELPs are extended to about 15 nm; i.e., the distance of the onset of steric repulsive interactions. This interaction distance decreased significantly with increasing salt concentration. To further quantify this behavior, we fitted force extension data on approach to a decaying exponential relation of the form,

$$F(x) = A \cdot \exp(-kD), \tag{S7}$$

where F is the force, A is a constant, D is the separation, and k is the inverse decay length. The decay length, plotted as a function of salt concentration (inset in Fig. S6), is a convenient measure for ELP conformation on the surface, and decreases linearly with increasing salt concentration. A qualitatively similar behavior was found when measuring the steric force response as a function of increasing temperature (data not shown).

Figure Captions

Figure S1: Separation residual plots from least-squares fitting of a force-extension curves using the FJC model for ELP. Also shown are the variance functions (Eq.1S) obtained from weighted least-squares shown as $\pm 2\sigma\sqrt{V_{d(f)}}$.

Figure S2: Drag force plotted as a function of pulling velocity. Solid lines are linear fits to the data and their slopes yield the coefficient $C\mu$ in Eq. 5S.

Figure S3: Hydrodynamic drag force correction applied to a typical force-extension profile obtained for ELP1-180 in PBS buffer solution.

Figure S4: Spring constant sensitivity analysis for ELP1-180 in a) deionized H₂O measured and b) PBS with 1.5 M NaCl added, at T = 25 °C. Each histogram in the figures shows a Kuhn length distribution corresponding to spring constants in the range between 80 - 120% K_c .

Figure S5: Effect of solvent on the areas calculated from the normalized force-extension curves after smoothing using the shared curve model for ELP1-180 in PBS and PBS+1.5 M NaCl.

Figure S6: Force separation curves for end-grafted ELP in PBS plotted for several levels of salt addition. For ELP in PBS buffer the interactions are purely repulsive, whereas with increasing salt concentration a secondary minimum occurs. This minimum is shifted to lower separations with increasing salt concentration. Each curve shown is averaged from 15 force curves at a given salt concentration. Inset: Decay length plotted as a function of salt concentration.

References

- (1) Hugel, T.; Grosholz, M.; Clausen-Schaumann, H.; Pfau, A.; Gaub, H.; Seitz, M. *Macromolecules* **2001**, *34*, 1039-1047.
- (2) Janshoff, A.; Neitzert, M.; Oberdorfer, Y.; Fuchs, H. *Angew. Chem., Int. Ed.* **2000**, *39*, 3213-3237.
- (3) Zhang, W.; Zhang, X. *Prog. Polym. Sci.* **2003**, *28*, 1271-1295.
- (4) Mardia, K. V.; Jupp, P. E. *Directional statistics*; John Wiley & Sons Chichester, 2000.
- (5) Efron, B.; Tibshirani, R. *An Introduction to the Bootstrap* New York, 1993.
- (6) Eckel, R.; Ros, R.; Ros, A.; Wilking, S. D.; Sewald, N.; Anselmetti, D. *Biophys. J.* **2003**, *85*, 1968-1973.
- (7) Haupt, B. J.; Senden, T. J.; Sevick, E. M. *Langmuir* **2002**, *18*, 2174-2182.
- (8) Rief, M.; Gautel, M.; Oesterhelt, F.; Fernandez, J. M.; Gaub, H. E. *Science* **1997**, *276*, 1109-1112.
- (9) Sader, J. E.; Larson, I.; Mulvaney, P.; White, L. R. *Rev. Sci. Instrum.* **1995**, *66*, 3789-3798.
- (10) Maeda, N.; Senden, T. J. *Langmuir* **2000**, *16*, 9282-9286.
- (11) Hutter, J. L.; Bechhoefer, J. *Rev. Sci. Instrum.* **1993**, *64*, 1868-1873.
- (12) Cleveland, J. P.; Manne, S.; Bocek, D.; Hansma, P. K. *Rev. Sci. Instrum.* **1993**, *64*, 403-405.

Figure S1

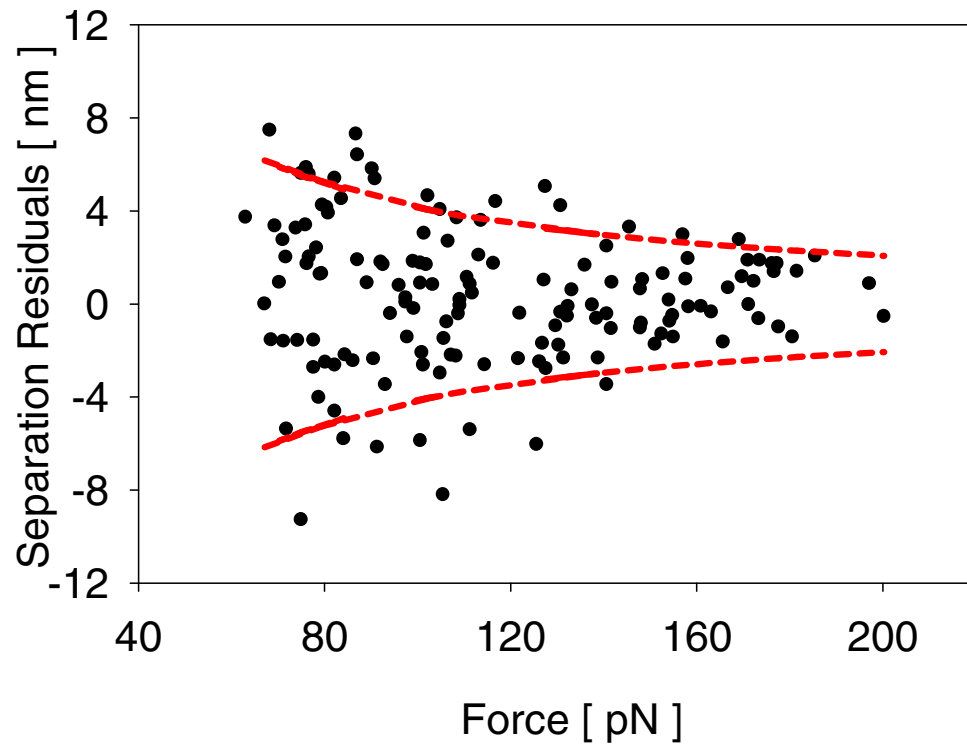


Figure S2

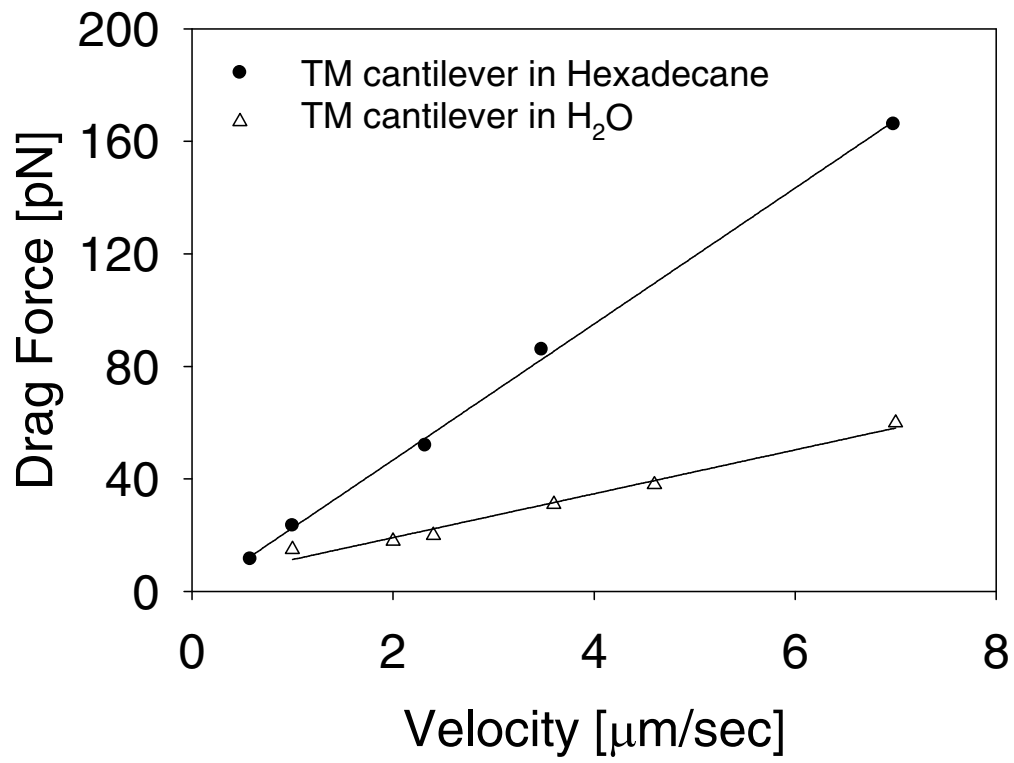


Figure S3

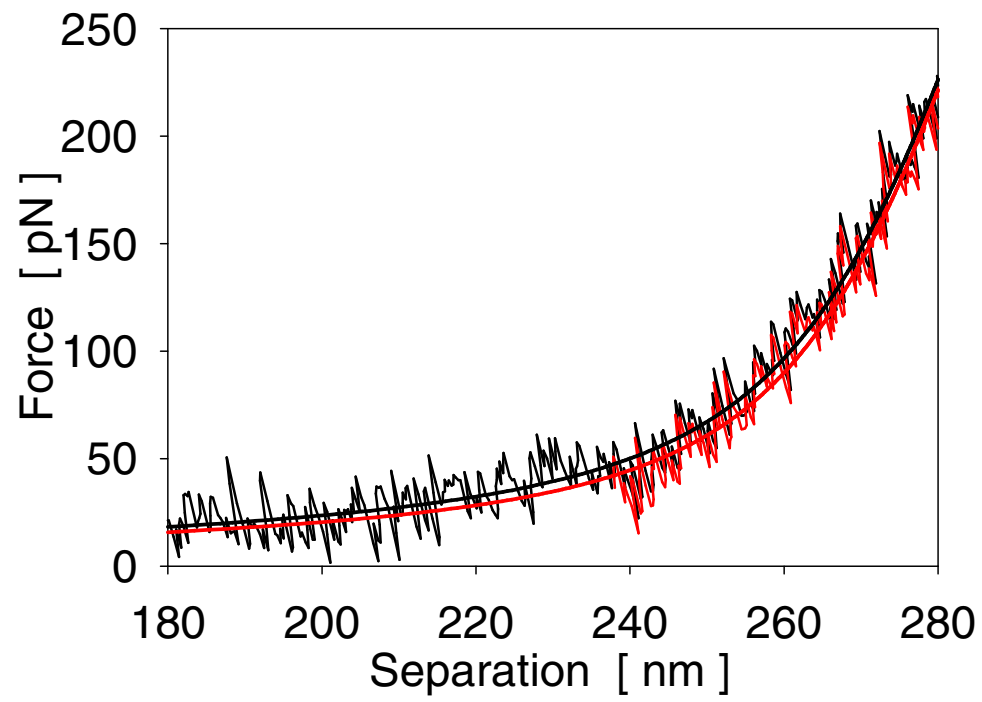


Figure S4

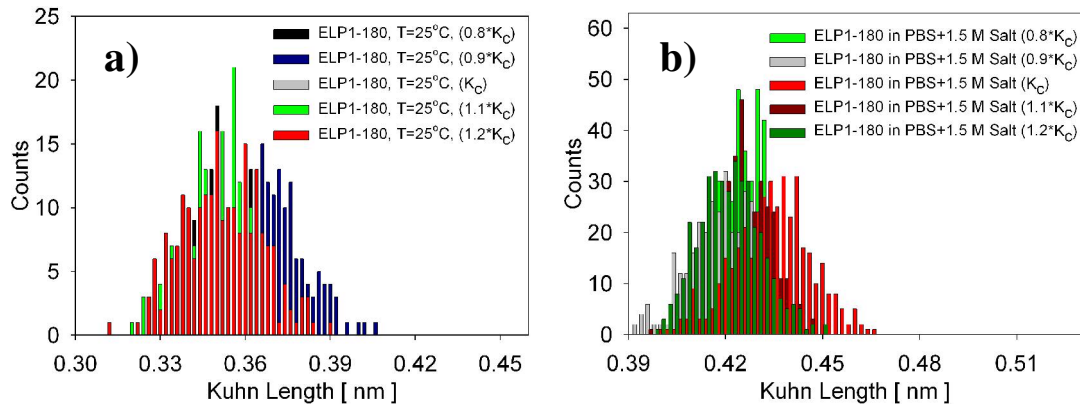


Figure S5

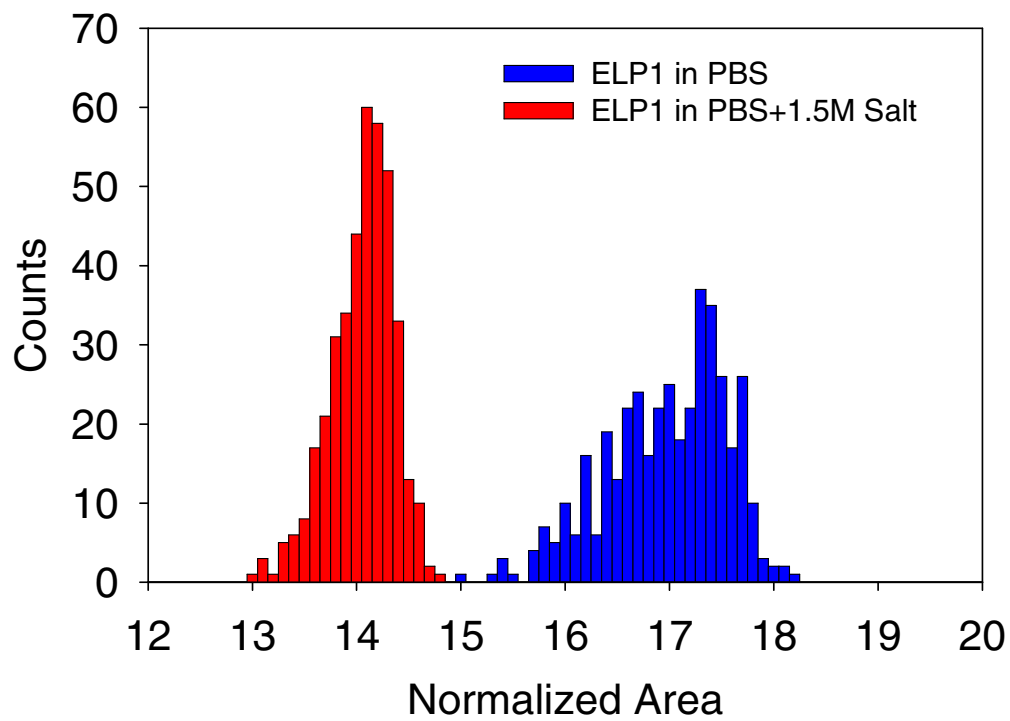


Figure S6

